

CHORUS

This is the accepted manuscript made available via CHORUS. The article has been published as:

Kondo hybridization and quantum criticality in β -YbAlB₄ by laser ARPES

Cédric Bareille, Shintaro Suzuki, Mitsuhiro Nakayama, Kenta Kuroda, Andriy H. Nevidomskyy, Yosuke Matsumoto, Satoru Nakatsuji, Takeshi Kondo, and Shik Shin

Phys. Rev. B **97**, 045112 — Published 10 January 2018

DOI: [10.1103/PhysRevB.97.045112](https://doi.org/10.1103/PhysRevB.97.045112)

Kondo hybridization and quantum criticality in β -YbAlB₄ by laser-ARPES

Cédric Bareille,^{1,*} Shintaro Suzuki,¹ Mitsuhiro Nakayama,¹
Kenta Kuroda,¹ Andriy H. Nevidomskyy,² Yosuke Matsumoto,³
Satoru Nakatsuji,^{1,4} Takeshi Kondo,¹ and Shik Shin¹

¹*ISSP, University of Tokyo, Kashiwa 277-8581, Japan*

²*Department of Physics and Astronomy & Center for Quantum Materials,
Rice University, Houston, Texas 77005, USA*

³*Max Planck Institute for Solid State Research,
Heisenbergstrasse 1, Stuttgart 70569, Germany*

⁴*CREST, Japan Science and Technology Agency (JST),
4-1-8 Honcho Kawaguchi, Saitama 332-0012, Japan*

Abstract

We report the first angle-resolved photoemission (ARPES) study of β -YbAlB₄, which is known to harbor unconventional quantum criticality (QC) without any tuning. We directly observe a quasiparticle peak (QP), emerging from hybridization, with unified binding energy and onset of coherence conformed with previously observed reduced Kondo scale at about 40 K. Consistency with earlier study of carriers in β -YbAlB₄ by Hall effect strongly suggest, from their own conclusions, this QP to be responsible for the QC in β -YbAlB₄. Comparison with the sister polymorph α -YbAlB₄, which is not quantum critical at ambient pressure, further support this result. Indeed, no hybridization could be observed within our instrumental resolution in this locally isomorphic system, while the conduction band we observe is essentially the same as in β -YbAlB₄. We therefore claim that we identified by ARPES the carriers responsible for the QC in β -YbAlB₄. The observed dispersion and the underlying hybridization of this QP are discussed in the context of existing theoretical models.

PACS numbers: 71.18.+y, 71.27.+a

I. INTRODUCTION

The formation of a non-magnetic Kondo-singlet ground-state commonly provides a description of heavy Fermi liquid (FL) in intermetallics rare-earth compounds. It emerges below the Kondo temperature T_K , from the screening of the local moments of f -orbitals by conduction electrons, which accompanies the onset of coherence of a quasiparticle (QP) peak binding at $k_B T_K$: the Kondo resonance peak¹. When external parameters are accurately tuned, numerous heavy fermion systems deviate from this normal FL. In the conventional scenario, spin density waves instabilities induce such non-FL behavior by driving the system to the critical regime of a magnetic quantum transition².

In β -YbAlB₄, quantum criticality (QC) has been observed below about 4 K at zero magnetic field and ambient pressure³, away from any magnetic order⁴. It, therefore, cannot be cast in this usual picture of magnetic instability. Moreover it shows an unexpected (T/B) -scaling^{3,5} and unusual critical exponents⁶ which challenge theoretical descriptions. Diverse works⁷⁻¹² attempt to model this unconventional QC, without any possible consensus. Although the FL behavior is recovered with a moderate magnetic field, its description and formation in terms of Kondo screening are still poorly understood. Indeed, despite a large Kondo scale $T_K \approx 250$ K, incoherent skew scattering is observed down to $T_{\text{coh}} \approx 40$ K¹³ and magnetic moments are still present as low as $T^* \approx 8$ K⁵. Kondo lattice behavior finally sets only below T^* . Advanced analysis of Hall effect measurements shed some light by the identification of two different components of carriers with distinct Kondo scales¹³, which we call carriers a and carriers b for convenience. Carriers a govern the longitudinal transport with T_K as Kondo scale and a relatively high carrier density n_a^{hall} , while carriers b have a low carrier density n_b^{hall} with electron-like character and gains coherence below a second Kondo scale at T_{coh} . Conclusion from Hall effect measurements further points carriers b as responsible of both Kondo lattice and QC behaviors below T^* ¹³. Nevertheless details about the emergence of these carriers and about the underlying Kondo physics are still lacking.

In the present article, we take advantage of the apparent location of the QC at zero magnetic field, without tuning of any control parameter³, to directly probe QP in β -YbAlB₄ by high-resolution laser-ARPES. In order to highlight any relation between microscopic observations and the QC, we also perform ARPES measurements on the sister compound α -YbAlB₄, whose structure is sketched alongside that of β -YbAlB₄ in Figure 1(a). This

locally isomorphic compound exhibits very similar behaviors and temperature scales, however unlike β -YbAlB₄, it does not display QC, developing instead a heavy Fermi liquid¹⁴. Moreover, it has been shown that the magnetization in β -YbAlB₄ can be separated into two components: the QC component and a heavy Fermi-liquid component similar to that in α -YbAlB₄⁵. Thus, α -YbAlB₄ is a perfect control system to study the unconventional criticality in β -YbAlB₄.

Our measurements reveal the hybridization between the crystal-field split heavy Yb f -electron bands and a light conduction band in β -YbAlB₄. The resulting electron-like QP has unified binding energy and onset of coherence of about 4 meV, consistent with carriers b highlighted by Hall measurements as responsible for the QC. By contrast, we find almost no or very weak hybridization in the sister α -phase, while the dispersion of the conduction band is very similar between the two phases. Our results strongly suggest the importance of the Kondo hybridization for the microscopic mechanism behind the QC in β -YbAlB₄.

II. METHODS

High quality single crystals were grown by using the Al-flux method as described in the literature¹⁵. The excess Al flux was etched by a water solution of sodium hydroxide. All ARPES measurements were performed with a SES R4000 analyzer, in a chamber shielded from magnetic field by mu-metal. Clean surfaces were obtained by cleaving crystals along the (a, b) -plane in ultra-high vacuum (below 5×10^{-11} Torr). Measurements in the (100) -plane were carried out at the 1-cubed end-station at Helmholtz-Zentrum Berlin, by tuning the photon energy from 24 eV to 120 eV, thanks to the synchrotron radiation of the BESSY-II facility. The temperature was about 1 K and the overall resolution of about 10 meV. Measurements in the (001) -plane for both β - and α -phases, were realized with a 6.994 eV laser at the ISSP, at a temperature of 5 K, with an overall resolution of about 3 meV. Data from β -YbAlB₄ were measured with circular polarized light, while data from α -YbAlB₄ were measured with linear horizontal polarized light. Nevertheless, as the Supplemental Figure S1 shows¹⁶, measurements with linear horizontal polarized light gives similar results as with circular polarized light. Thus, this difference does not affect our observations. Treatments by 2D curvature of some spectra of this work are performed following the method described in Ref. 17.

III. RESULTS

The β -YbAlB₄ crystal has an orthorhombic structure¹⁵; Figure 1(b) schematizes the corresponding Brillouin-zone (BZ). Samples were cleaved along the (a, b) -plane to perform photoemission. Figure 1(c) shows the edges of the BZ overlaid on a mapping in the (100) -plane, 50 meV below the Fermi level, while the dispersion along normal emission, Γ -Z line, is displayed on Figure 1(d). Conversion into momentum space was made in the frame of the nearly free electron final state approximation¹⁸. The inner potential was determined to be $V_0 \approx 22$ eV thanks to the point-group symmetry and periodicity, with, as a main indication, a hole-like band centered on the Z point, depicted by the gray parabola in panel (d) and the gray ellipse in panel (c). Also visible in panel (d) is a nearly flat band bounded at about 100 meV below E_F – it is a part of the Yb²⁺ $|J = 7/2\rangle$ multiplet, which has been previously observed by X-ray photoemission spectroscopy¹⁹. Complete investigation and discussion over the full three-dimensional BZ will be part of a future work. Here, we will focus instead on the results from laser-ARPES, which while being more restricted in \mathbf{k} -space, offers very high resolution and intensity.

Given the laser photon energy $h\nu = 6.994$ eV, the available BZ cut is depicted by the lower purple circle in Fig. 1(c), which crosses the Γ -Z line less than 0.2 \AA^{-1} below the Z point, named \tilde{Z} for convenience. Measurements with photon energy $h\nu = 54$ eV reaches an equivalent position along the Γ -Z line (see higher purple circle in Fig. 1c). The dispersive hole-like band with the top bound at about -45 meV, as well as the flat band at about -90 meV were observed using both the light source with photon energy $h\nu = 54$ eV [see panels (c, d)], as well as with the laser in panel (e), thus providing a calibration of our laser-ARPES. In what follows, we focus on the bands above $E > -40$ meV, observable thanks to laser-ARPES, and compare them to our measurements on α -YbAlB₄.

We investigate the vicinity of E_F with the stack of energy distribution curves (EDCs), Figure 2(a), extracted along k_y , i.e. along the analyzer slit, with $k_x = 0$ (full gray line A on Fig. 2(b)). We observe three dispersions; they can be modeled by a light electron-like band with $m^* \approx 3 m_e$ and the band bottom of ≈ 20 meV below E_F , which hybridizes and forms anti-crossings with two flat bands, a first one around -4 meV and a second one around -13 meV (thin dashed lines in Fig. 2(c) and 2(d)). These two flat bands, separated by 9 meV are consistent with the crystal electric field of about 80 K, extracted from fitting the

magnetic susceptibility²⁰. From this fitting and local symmetry considerations detailed in Ref. 20, the two flat bands can then be identified as the ground-state $J_z = \pm 5/2$ ($|\pm 5/2\rangle$), at -4 meV, and the first crystal-field excited state, dominated by $J_z = \pm 3/2$ ($|\pm 3/2\rangle$), at -13 meV, of the $J = 7/2$ Yb multiplet. In Figure 2(c), solid lines are the results of fitting to the hybridization model with a constant hybridization function $V \approx 4$ meV. The first anti-crossing at -5 meV is nicely fitted, and forms an electron-like QP band (blue line in Fig. 2(c)) bound at about 4 meV below E_F . This energy scale, one order of magnitude smaller than $T_K \approx 250$ K, is consistent with the expectation from previous experimental observations^{13,14} of a reduced Kondo scale at $T_{\text{coh}} \approx 40$ K (≈ 3.4 meV).

The temperature dependence of EDCs in Figure 3 confirms the relation between the QP peak and T_{coh} . Panels (a) and (b) shows EDCs from 5 K to 60 K at the inner ($k_y = 0 \text{ \AA}^{-1}$) and outer ($k_y = 0.17 \text{ \AA}^{-1}$) sides of the anti-crossing respectively. Same EDCs divided by the Fermi-Dirac step are displayed at the bottom of these two panels. For both, the QP peak slowly disappears as the temperature goes up. It is clearer on the outer EDCs where the peak intensity suddenly drops from 30 K to 40 K. The peak is totally restored by cooling back down (light blue EDC), showing that our observations are not due to a surface degradation. For both inner and outer peaks, intensity integrated along the shade area (see panels (a) and (b) respectively) of EDCs divided by the Fermi-Dirac step are displayed against the temperature on panel (c), relatively to the value at 60 K. Both peaks slowly drop when temperature crosses T_{coh} . It is worth to emphasize that, to our knowledge, it is the first direct and fully resolved observation by ARPES of a Kondo-like hybridization with unified binding energy, onset of coherence and Kondo scale. While a similar observation has been reported on YbRh_2Si_2 , both QP peak and hybridization gap were not fully resolved²¹.

Nevertheless, here, the second anti-crossing at $E \approx -15$ meV is badly reproduced by the constant hybridization model (magenta line in Fig. 2(c)). By taking a \mathbf{k} -dependent hybridization proposed theoretically^{8,20}, we obtain a more satisfying fit, as shown by the magenta line in Figure 2(d). The fitting parameters of both models are detailed in the Supplemental Materials¹⁶. Finally, the hybridization with the $|\pm 5/2\rangle$ level at about -4 meV results in the small electron-like QP peak (blue line in panels (c) and (d) of Fig. 2), which crosses the Fermi level at $k_{\text{F1}}^\beta \approx 0.09 \text{ \AA}^{-1}$ and has a mass of about $3 m_e$ at E_F . It forms a quite isotropic Fermi sheet, as can be seen via the in-plane mapping at E_F in Figure 2(b) (blue circle). The size, mass and isotropy of this small pocket are compatible with the observations

by quantum oscillations on β -YbAlB₄²².

It should be noted that, along the $\langle 010 \rangle$ direction, the $|\pm 5/2\rangle$ level crosses E_F at about $k_{F2}^\beta \approx 0.25 \text{ \AA}^{-1}$. This second Fermi-momentum is exhibited by red arrows on the Fermi-mapping, Figure 2(b), as well as on the cut along the $\langle 010 \rangle$ direction, Figure 2(e). Blue, red and pink full lines are guide to the eyes for the same dispersions as Figure 2(d). The observation of a second Fermi-momentum implies an overlapping of the blue and red hybridized bands, on the Figure 2(e). In order to account for it, we need to introduce a small dispersion to the $|\pm 5/2\rangle$ level in our model, corresponding to a mass $m_f^* \approx 70 m_e$ in the $\langle 010 \rangle$ direction. This very large mass makes it difficult to be observed by quantum oscillations.

Carrier density can be estimated at the $T = 0$ limit assuming spherical Fermi sheets by $n = k_F^3/3\pi^2$ ²³. Before hybridization, the little conduction band has a density of $n_c^{\text{ARPES}} \approx 7.4 \times 10^{25} \text{ m}^{-3}$. It is of the same order as the value estimated from Hall measurements¹³ of carriers b at $T = 140 \text{ K}$ (i.e. above the integration of f -electron to the Fermi surface): $n_b^{\text{hall}}(T = 140 \text{ K}) \approx 16 \times 10^{25} \text{ m}^{-3}$. Below T_{coh} , carrier density could not be accurately extracted from the Hall measurements. Yet, estimation of the density of the two Fermi sheets from our measurements (i.e. including f -electrons) $n^{\text{ARPES}} \approx 55 \times 10^{25} \text{ m}^{-3}$ is still one order of magnitude smaller than the density of carriers a pointed as main contribution to the transport by Hall effect measurements, estimated at 50 K to $n_a^{\text{hall}}(T = 50 \text{ K}) \approx 416 \times 10^{25} \text{ m}^{-3}$. Therefore, carriers of β -YbAlB₄ observed here thanks to the high-resolution of laser-ARPES, match carriers b pointed as responsible for both Kondo lattice and QC behaviors below T^* by Hall effect measurements. Specifically, they are of electron-like character, gain coherence below T_{coh} and have low carrier density. From these evidences, we argue that the observed Fermi sheets and the underlying Kondo hybridization are closely related to both Kondo lattice and QC behaviors below T^* .

To verify our claim, we now look at the electronic structure of the sister compound α -YbAlB₄ in the vicinity of E_F . Figure 4(a) displays the laser-ARPES curvature spectra along the $\langle 100 \rangle$ direction, where mainly two features are visible: an almost flat band and a light electron-like band dispersing all the way up to E_F . The former is revealed by fitting the peaks in the EDCs (open circles) at about -13 meV below E_F . The dispersive electron-like band is better seen by fitting the peaks from the momentum distribution curves (MDCs) (full circles in Fig. 4(a,b)) down to -12 meV ; the two peaks are difficult to distinguish at higher binding energies. The peaks are directly visible on the stack of MDCs, Figure 4(b).

This light dispersion crosses E_F at $k_F^\alpha \approx 0.13 \text{ \AA}^{-1}$.

In Figure 5(a), we compare the two aforementioned bands with the ones observed in β -YbAlB₄. Intriguingly, they are identical to the dispersive electron-like band and the flat $|\pm 3/2\rangle$ band derived from the \mathbf{k} -dependent hybridization model used for β -YbAlB₄, copied onto panel (a) with dashed lines. On the other hand, the $|\pm 5/2\rangle$ level is seemingly not observed in α -YbAlB₄. A peak is visible at $k = 0$, however it is very limited in momentum space and may correspond to a different conduction band. We directly compare the EDCs from β - and α -YbAlB₄ in Figure 5(b), in red and green lines respectively. Red open arrows show the $|\pm 5/2\rangle$ level as a peak on the β -YbAlB₄ EDCs. On α -YbAlB₄, only shoulders are visible. When divided by the Fermi-Dirac step, these shoulders disappear, and no peak is left, thus indicating the absence of the $|\pm 5/2\rangle$ level in our data on α -YbAlB₄. On the other hand, one would expect the crystal field splitting to be very similar between these two locally isomorphic phases, and the absence of the $|\pm 5/2\rangle$ level in our data could be a result of a bad sample surface quality, which especially may affect the conclusions so close to E_F . What can be said with certainty, however, is that we do not observe any sign of hybridization between either of the flat Yb $4f$ levels and the conduction electron bands in α -YbAlB₄, within our instrumental resolution. Indeed, the light electron-like band disperses straight through the -4 meV energy to cut through E_F , while no gap is visible at about -13 meV where one would expect the second anti-crossing with Yb $|\pm 3/2\rangle$ level. This is evidenced by the EDCs in Fig. 5(b): on α -YbAlB₄, the $|\pm 3/2\rangle$ level (full green arrows) is at the same position on both $k = 0$ and $k = \pm 0.15 \text{ \AA}^{-1}$, in clear contrast with EDCs on β -YbAlB₄.

IV. DISCUSSION

The apparent absence of the Kondo hybridization in the ARPES data on α -YbAlB₄, in contrast to β -YbAlB₄, further supports that the hybridization and emerging QP peak play a crucial role in the unconventional quantum criticality observed in the latter compound. Moreover, our analysis shows that the heavy dispersions of β -YbAlB₄ are best fitted with a \mathbf{k} -dependent hybridization function, as put forward by the theory of the critical nodal metal⁸. It is important to note however that for this model to explain the observed T/B scaling in β -YbAlB₄, the renormalized position \tilde{E}_f of the ground state $|\pm 5/2\rangle$ doublet must be pinned

at the Fermi level. It is therefore difficult to unequivocally corroborate the theoretical model, in its original form, based on our ARPES data. It follows from our ARPES analysis that this doublet actually crosses the Fermi level at the wavevector $k_{\text{F}2}^{\beta} \approx 0.25 \text{ \AA}^{-1}$ and has an intrinsic bandwidth, characterized by a heavy quasi-particle mass $m_f^* \sim 70 m_e$. Clearly, this situation is more complex than in the nodal metal theory of Ref. 8, where the $|\pm 5/2\rangle$ doublet was assumed to be perfectly flat, in other words the Yb-Yb electron hopping was neglected. In this situation, it could be possible for a portion of the nodal line to be bound at the Fermi level. Since our present observations already support the \mathbf{k} -dependent hybridization, investigating the dispersion of the $|\pm 5/2\rangle$ doublet along the c -axis would be desirable.

We note that the observation of the second Fermi-momenta $k_{\text{F}2}^{\beta}$ may also be consistent with the model of deconfinement of the f -electrons²⁴, whose application to β -YbAlB₄ has been proposed by Hackl and Thomale¹⁰. In this model, $k_{\text{F}2}^{\beta}$ hosts the critical fluctuations, while carriers at $k_{\text{F}1}^{\beta}$, labeled ‘cold’, exhibit a FL behavior. Naively, this is compatible with the similar observation of the Fermi-momenta k_{F}^{α} in the FL of α -YbAlB₄. Nevertheless, we did not observe any direct sign of such deconfinement in our data; from the ARPES point of view, measurements at lower temperature is necessary to follow the coherence of the $|\pm 5/2\rangle$ and to settle this question. In fact, previous electrical and thermal transport measurements²⁵ discards this scenario by highlighting a discrepancy with the expectation advanced by Hackl and Thomale of a characteristic maximum in the Wiedemann-Franz ratio¹⁰.

Finally, we note that the band structure observed in the present ARPES measurement is consistent with the theory of the electron spin resonance (ESR) in β -YbAlB₄ by Ramires *et al.*²⁶. Indeed, in addition to the unconventional QC, β -YbAlB₄ shows a singular ESR signal, characterized by hyperfine satellites at low temperature, and by the constancy of the ESR signal intensity²⁷. The work of Ramires *et al.* reproduces first the hyperfine satellites by including Yb atoms with nonzero nuclear spin into the Kondo screening, and then the constancy of the signal intensity by a crystal electric field comparable to the Kondo hybridization strength²⁶. The band structure we observe in ARPES, with the hybridization of about 4 meV of the same order as the crystal electric field ~ 9 meV, directly confirms the theoretical assumption in Ref. 26. Additionally, the absence of the Kondo-like hybridization in our ARPES measurements of α -YbAlB₄, along with the absence of hyperfine satellites in its ESR signal²⁸ tends to reinforce this model.

V. CONCLUSIONS

In conclusion, we report the first ARPES study of both β - and α -YbAlB₄, with the key observation of a Kondo-like hybridization between the crystal-field split Yb f -levels and an electron-like conduction band in β -YbAlB₄. The crystal-field splitting inferred from our ARPES data has a magnitude of ~ 9 meV, in good agreement with previous estimation²⁰. Based on this agreement, we are able to use the theoretical arguments to identify the low-lying heavy band at -4 meV below E_F as the ground state $|J_z = \pm 5/2\rangle$ doublet, and the band at -13 meV as the first excited crystal-field state, dominated by $|J_z = \pm 3/2\rangle$ of the Yb $J = 7/2$ multiplet.

The observed hybridization gives rise to a small electron-like QP pocket whose size and effective mass are consistent with quantum oscillations measurements²², together with a heavier Fermi sheet as the hybridized bands overlap in energy. Importantly, this QP exhibits unified binding energy and onset of coherence of about 4 meV, conform with the earlier indications of a reduced Kondo coherence temperature $T_{\text{coh}} \approx 40$ K^{13,14}. Thus, as evidenced by the Hall effect measurements, it is indeed these Fermi sheets that are responsible for both Kondo lattice and QC behaviors below T^* ¹³.

Measurements of α -YbAlB₄ further support our conclusion. Indeed, in α -YbAlB₄, we similarly observe the electron-like conduction band and the flat band at -13 meV below E_F , which we also identify as the $|\pm 3/2\rangle$ state. However, where β -YbAlB₄ shows two anti-crossings of Yb $4f$ levels with the dispersive conduction band, the bands in the α -phase do not show, within our resolution, any apparent sign of hybridization. This dichotomy strongly suggests that this hybridization plays a crucial role in the unconventional quantum criticality in β -YbAlB₄, whereas α -YbAlB₄ is not critical.

While our observations cannot sharply infer the microscopic mechanism behind the non-Fermi-liquid behavior in β -YbAlB₄, they provide an important insight for the future experimental and theoretical investigations. As we already mentioned, further ARPES measurements at lower temperature, and in wider regions of the Brillouin-zone, will have the potential to shed more light on this intriguing quantum critical behavior.

ACKNOWLEDGMENTS

We thank S. Burdin, S. Watanabe and D. Malterre for helpful discussions. We thank P. Zhang for sharing his procedure to perform 2D curvature. We thank D. Evtushinsky and E. Rienks for their precious support on the 1-cubed end-station. We thank HZB for the allocation of synchrotron radiation beamtime and thankfully acknowledge the financial support by HZB. This work was supported by CREST, Japan Science and Technology Agency, Grants-in-Aid for Scientific Research (Grant Nos. 16H02209, 25707030, 26105002), by Grants-in-Aid for Scientific Research on Innovative Areas “J-Physics” (Grant Nos. 15H05882 and 15H05883) and Program for Advancing Strategic International Networks to Accelerate the Circulation of Talented Researchers (Grant No. R2604) from the Japanese Society for the Promotion of Science. A.H.N. was supported by the grant no. DMR-1350237 from the U.S. National Science Foundation.

* bareille@issp.u-tokyo.ac.jp

- ¹ A. C. Hewson, *The Kondo problem to Heavy Fermions*, edited by C. U. Press (1993).
- ² H. v. Löhneysen, A. Rosch, M. Vojta, and P. Wölfle, *Rev. Mod. Phys.* **79**, 1015 (2007).
- ³ Y. Matsumoto, S. Nakatsuji, K. Kuga, Y. Karaki, N. Horie, Y. Shimura, T. Sakakibara, A. H. Nevidomskyy, and P. Coleman, *Science* **331**, 316 (2011).
- ⁴ T. Tomita, K. Kuga, Y. Uwatoko, P. Coleman, and S. Nakatsuji, *Science* **349**, 506 (2015).
- ⁵ Y. Matsumoto, K. Kuga, Y. Karaki, Y. Shimura, T. Sakakibara, M. Tokunaga, K. Kindo, and S. Nakatsuji, *Journal of the Physical Society of Japan* **84**, 024710 (2015).
- ⁶ S. Nakatsuji, K. Kuga, Y. Machida, T. Tayama, T. Sakakibara, Y. Karaki, H. Ishimoto, S. Yonezawa, Y. Maeno, E. Pearson, G. G. Lonzarich, L. Balicas, H. Lee, and Z. Fisk, *Nature Physics* **4**, 603 (2008).
- ⁷ T. Misawa, Y. Yamaji, and M. Imada, *Journal of the Physical Society of Japan* **78**, 084707 (2009).
- ⁸ A. Ramires, P. Coleman, A. H. Nevidomskyy, and A. M. Tsvelik, *Phys. Rev. Lett.* **109**, 176404 (2012).
- ⁹ J. H. Pixley, S. Kirchner, K. Ingersent, and Q. Si, *Phys. Rev. Lett.* **109**, 086403 (2012).

- ¹⁰ A. Hackl and R. Thomale, *Phys. Rev. B* **83**, 235107 (2011).
- ¹¹ S. Watanabe and K. Miyake, *Journal of the Physical Society of Japan* **83**, 103708 (2014).
- ¹² V. R. Shaginyan, A. Z. Msezane, K. G. Popov, J. W. Clark, V. A. Khodel, and M. V. Zverev, *Phys. Rev. B* **93**, 205126 (2016).
- ¹³ E. C. T. O’Farrell, Y. Matsumoto, and S. Nakatsuji, *Phys. Rev. Lett.* **109**, 176405 (2012).
- ¹⁴ Y. Matsumoto, K. Kuga, T. Tomita, Y. Karaki, and S. Nakatsuji, *Phys. Rev. B* **84**, 125126 (2011).
- ¹⁵ R. T. Macaluso, S. Nakatsuji, K. Kuga, E. L. Thomas, Y. Machida, Y. Maeno, Z. Fisk, and J. Y. Chan, *Chemistry of Materials* **19**, 1918 (2007).
- ¹⁶ See Supplemental Material at [link] for a comparison, side by side, of laser-ARPES spectra of β -YbAlB₄ with linear polarized and circular polarized light, for examples of EDCs fits performed in this work, for raw data of Figures 2 and 4, and for details of hybridization models used in Figures 2(c, d).
- ¹⁷ P. Zhang, P. Richard, T. Qian, Y.-M. Xu, X. Dai, and H. Ding, *Review of Scientific Instruments* **82**, 043712 (2011).
- ¹⁸ A. Damascelli, *Physica Scripta* **2004**, 61 (2004).
- ¹⁹ M. Okawa, M. Matsunami, K. Ishizaka, R. Eguchi, M. Taguchi, A. Chainani, Y. Takata, M. Yabashi, K. Tamasaku, Y. Nishino, T. Ishikawa, K. Kuga, N. Horie, S. Nakatsuji, and S. Shin, *Phys. Rev. Lett.* **104**, 247201 (2010).
- ²⁰ A. H. Nevidomskyy and P. Coleman, *Phys. Rev. Lett.* **102**, 077202 (2009).
- ²¹ S.-K. Mo, W. S. Lee, F. Schmitt, Y. L. Chen, D. H. Lu, C. Capan, D. J. Kim, Z. Fisk, C.-Q. Zhang, Z. Hussain, and Z.-X. Shen, *Phys. Rev. B* **85**, 241103 (2012).
- ²² E. C. T. O’Farrell, D. A. Tompsett, S. E. Sebastian, N. Harrison, C. Capan, L. Balicas, K. Kuga, A. Matsuo, K. Kindo, M. Tokunaga, S. Nakatsuji, G. Csányi, Z. Fisk, and M. L. Sutherland, *Phys. Rev. Lett.* **102**, 216402 (2009).
- ²³ N. W. Ashcroft and N. D. Mermin, *Physique des solides*, edited by E. Sciences (2002).
- ²⁴ T. Senthil, S. Sachdev, and M. Vojta, *Physica B: Condensed Matter* **359-361**, 9 (2005), proceedings of the International Conference on Strongly Correlated Electron Systems.
- ²⁵ M. L. Sutherland, E. C. T. O’Farrell, W. H. Toews, J. Dunn, K. Kuga, S. Nakatsuji, Y. Machida, K. Izawa, and R. W. Hill, *Phys. Rev. B* **92**, 041114 (2015).
- ²⁶ A. Ramires and P. Coleman, *Phys. Rev. Lett.* **112**, 116405 (2014).

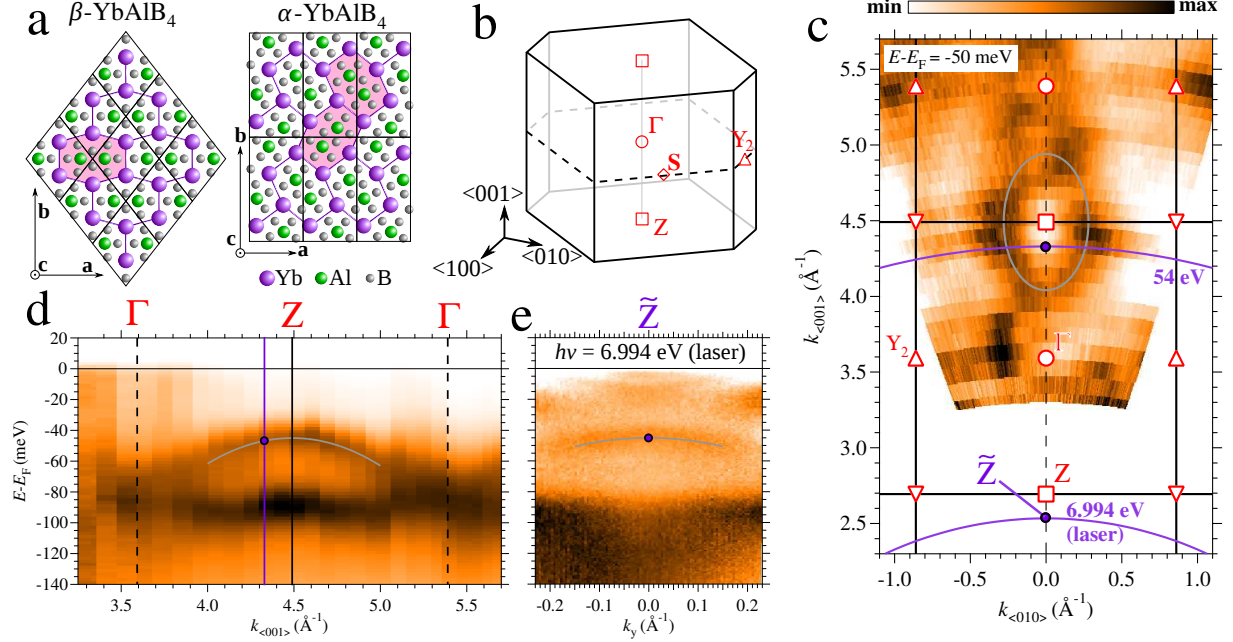


FIG. 1. a. Representation from the c -axis of the crystal structure of β -YbAlB₄(left) and α -YbAlB₄ (right). b. Brillouin-zone of β -YbAlB₄. c. Mapping in the (100)-plane, 50 meV below E_F . Full black lines are the edges of the BZ. Purple circles show the position reached with a light of $h\nu = 6.994$ eV and 54 eV. d. Dispersion at normal emission, i.e. along the $\langle 001 \rangle$ direction. e. Laser-ARPES spectra on β -YbAlB₄; $h\nu = 6.994$ eV.

²⁷ L. M. Holanda, J. M. Vargas, W. Iwamoto, C. Rettori, S. Nakatsuji, K. Kuga, Z. Fisk, S. B. Oseroff, and P. G. Pagliuso, *Phys. Rev. Lett.* **107**, 026402 (2011).

²⁸ L. M. Holanda, G. G. Lesseux, E. T. Magnavita, R. A. Ribeiro, S. Nakatsuji, K. Kuga, Z. Fisk, S. B. Oseroff, R. R. Urbano, C. Rettori, and P. G. Pagliuso, *Journal of Physics: Condensed Matter* **27**, 255601 (2015).

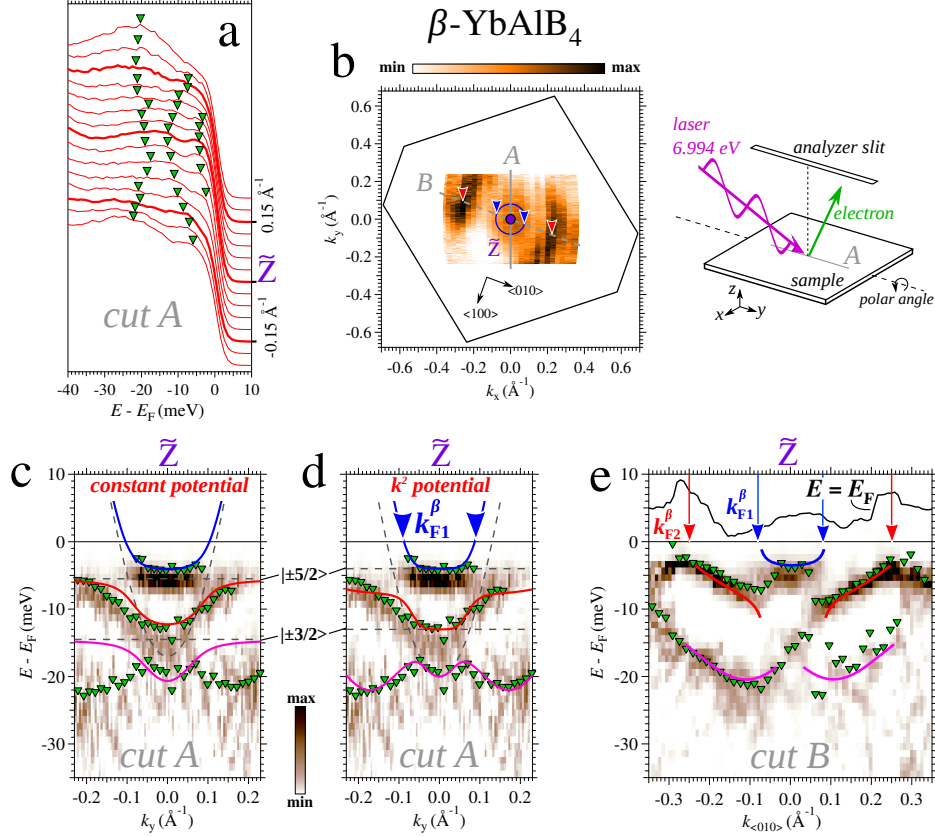


FIG. 2. Laser-ARPES on β -YbAlB₄. a. Stack of EDCs next to \tilde{Z} , along the full gray line A on panel (b). Green markers are peaks' position from EDCs, fitted by Voigts with a quadratic background and cut by a Fermi-Dirac step. Detailed fitting for $k_y = -0.15, 0$ and 0.15 \AA^{-1} are illustrated with the Supplemental Figure S2¹⁶. b. Fermi-surface mapping performed by tuning the polar angle. Sketch on the right illustrates the geometry of the measurements; The analyzer slit was oriented along the line A. The blue circle shows the little electron-like Fermi sheet, while the two red arrows show an outer Fermi sheet. Black lines are edges of the BZ. c. Curvature of the ARPES spectra measured along the slit of the analyzer (full gray line on panel (b)). Green markers are peaks' position as of panel (a). The blue, red and pink lines are the results of the modeling based on the constant hybridization of the original bands (represented by dashed black lines). d. Same as (c) with a \mathbf{k} -dependent nodal potential. See Supplemental Materials for the raw data (Fig. S3) and details of the hybridization models¹⁶. e. Curvature of the cut along the $\langle 010 \rangle$ direction (dashed gray line B on panel (b)). Green markers are peaks' position from EDCs fit. Full blue, red and pink lines are guide to the eyes. See Supplemental Figure S3 for the raw data¹⁶.

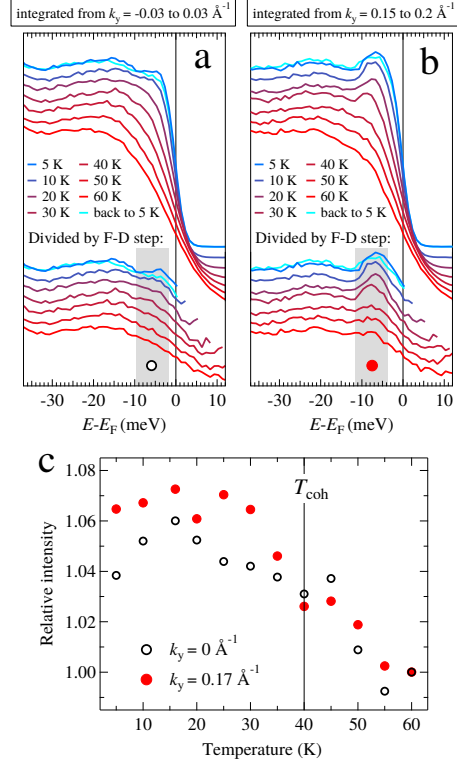


FIG. 3. Temperature dependence on β -YbAlB₄. a. EDCs at $k_y = 0 \text{ \AA}^{-1}$ from $T = 5 \text{ K}$ to 60 K . b. EDCs at $k_y = 0.17 \text{ \AA}^{-1}$ from $T = 5 \text{ K}$ to 60 K . (peak's intensity difference with EDC on Figure 2(a) is due to a slightly different orientation along the slit, as temperature dependence was performed on a different sample – see Supplemental Figure S1 for the corresponding color scale¹⁶) c. Intensity, relative to the value at 60 K , of the inner/outer peak from EDCs divided by the Fermi-Dirac step and integrated along the shade area of panel (a)/(b).

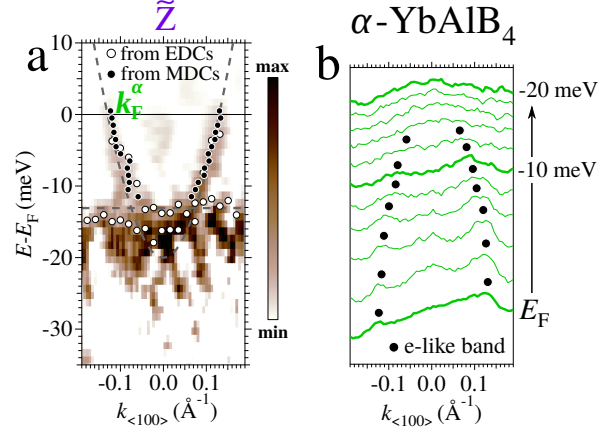


FIG. 4. Laser-ARPES on α -YbAlB₄. a. Curvature of the spectra along the $\langle 100 \rangle$ direction. Open and full circles are peaks' positions, extracted respectively from EDCs and MDCs. See Supplemental Figure S3 for the raw data¹⁶. b. MDCs stack of previous panel. Black markers are peaks' positions for the electron-like band. They were obtained by fitting MDCs by Voigts with a constant background.

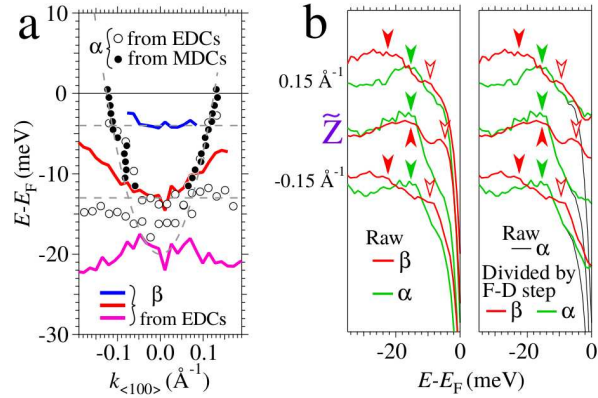


FIG. 5. a. MDCs and EDCs' fits (open and full markers) from α -YbAlB₄ compared to EDCs' fit on β -YbAlB₄ (blue, red and pink lines). The broken black lines denote the unhybridized electron-like conduction band and Yb 4*f* flat bands from the same model as in Figure 2. b. EDCs at $k = 0; \pm 0.15 \text{ \AA}^{-1}$ from β -YbAlB₄ (red) and α -YbAlB₄ (green). On the left panel is the raw, while the right panel shows the EDCs divided by the effective Fermi-Dirac step. Open arrows indicate the $|\pm 5/2\rangle$ level, while full arrows indicate the $|\pm 3/2\rangle$ level.